[American Journal of Science, Vol. 318, November, 2018, P. 949–968, DOI 10.2475/09.2018.04]

PHOTOCATALYTIC REDUCTION OF URANYL: EFFECTS OF ORGANIC LIGANDS AND UV LIGHT WAVELENGTHS

YOUNGJAE KIM*, MARIA C. MARCANO*, BRIAN R. ELLIS**, and UDO BECKER*,†

ABSTRACT. Although previous studies demonstrate the photochemical reduction of uranyl (UO_2^{2+}) in the presence of various organic compounds, the actual roles of organic molecules as ligands and electron donors during the photoreaction are poorly understood. In this study, photochemical reduction of uranyl is examined with respect to organic ligands as electron donors and complexing agents, the role of titanium oxide (TiO_2) nanoparticles as a photocatalyst, and the influence of UV light irradiation with emission peaks in the UV-A, UV-B, and UV-C ranges. Organic compounds with different binding affinities to uranyl such as acetate, ethylenediaminetetracetate (EDTA), oxalate, and hydroquinone were selected.

Uranyl solutions prepared with one organic compound in a 1:8 molar ratio were irradiated under anoxic and acidic conditions (O_2 < 1 ppm, pH 2.5). Uranyl removal by UV irradiation was better than 70 percent in the presence of oxalate and acetate, followed by hydroquinone (~ 45 %) and EDTA (~ 10 %). Uranyl removal was nearly constant at the UV-A, UV-B, and UV-C regions in the presence of acetate and oxalate whereas greater removal was observed in the EDTA and hydroquinone solutions exposed to UV-C and UV-A, respectively. These results reveal that uranyl reduction is mediated primarily by TiO_2 nanoparticles and is highly dependent on the electron-donor compound. Addition of acetate enhances the uranyl photoreaction in hydroquinone solution. Dissolved EDTA species act as good electron donors at limited EDTA concentrations (1:2 to 1:4 uranyl to EDTA ratios) but at higher concentrations (for example, 1:8), uranyl-EDTA complexes such as $[(UO_2^{2+})HEDTA]^-$ compete for the surface sites on the TiO_2 nanoparticles, hindering the photoreduction of uranyl. X-ray photoelectron spectroscopy (XPS) of the dried TiO_2 powder shows that more than 70 percent of uranium partitioned into the solid phase is present as reduced forms with oxidation states (V) and (IV). The U4f spectra of U partitioned to the solid phase from the photoreaction with acetate reveal the predominance of U(IV) over U(V), whereas U(V) is the dominant oxidation state as a result of the photoreduction with EDTA. Our results suggest that formation of uranium-ligand complexes plays a critical role in controlling the reactivity of uranyl species and the stability of reduced uranium species in the course of the photoreaction.

Key words: photocatalytic reduction of uranyl, anatase, rutile, P25, organic ligand, electron donor, UV wavelength

INTRODUCTION

The uranyl ion (UO_2^{2+}) is the most stable form of uranium with the oxidation number VI in natural settings such as soils and groundwater, and in waste mixtures (for example, in nuclear waste disposal sites). Although the mobility of uranyl can be retarded via sorption onto mineral and solid-waste surfaces as well as secondary mineralization (Yang and Davis, 2000; Kim and others, 2015), remobilization may occur due to complexation with dissolved ligands, thereby potentially spreading pollution. Ethylenediaminetetracetate (EDTA) is a chelating agent commonly used to increase the solubility of toxic and heavy metal ions including uranium as required for

* Department of Earth and Environmental Sciences, University of Michigan, 1100 North University Avenue, Ann Arbor, Michigan 48109-1005, USA
** Department of Civil & Environmental Engineering, University of Michigan, 1351 Beal Avenue, Ann Arbor, Michigan 48109-2125, USA
† Corresponding author: E-mail: ubecker@umich.edu

industrial applications such as chemical cleaning and decontamination operations. Oxalate is often found in nuclear waste repositories as it is produced by the decomposition of other organic compounds (Campbell and others, 1994). In addition, oxalic acid naturally occurs as a great source of protons and metal-complexing organic ligands that can make various metals (bio-) available in ecosystems (Gadd, 1999). Since uranyl forms strong complexes with these organics, their interactions are important in evaluating the mobility of uranyl in aqueous systems (Havel and others, 2002).

Because of increase in mobility, uranyl-organic complexes are difficult to treat using conventional techniques (Yang and Davis, 2000). One promising treatment approach is to couple metal reduction with photochemical oxidation of organic contaminants using a mineral catalyst. Anatase, a polymorph of titanium oxide (TiO_2), is known to be a robust and efficient mineral catalyst for such photochemical processes. Oxidation of various organic compounds such as EDTA, methanol, propanol, and acetate has been demonstrated to promote photocatalytic reduction of uranyl using anatase (Chen and others, 1999; Evans and others, 2004; Bonato and others, 2008; Salomone and others, 2015). There is a general consensus that the heterogeneous photoreduction of uranyl is hindered in the presence of dissolved oxygen and that uranyl can be reduced and precipitated as U(IV). However, the respective roles of organic molecules as ligands and electron donors upon this process have been barely investigated.

Upon the photochemical reduction of uranyl mediated by anatase, irradiation by photons with energies higher than its bandgap is necessary to excite the electron (e^-) from the valence band into the conduction band. As a result, a hole (h^+) is generated in the valence band. In order to overcome the bandgap of anatase (3.2 eV), the wavelength of electromagnetic radiation must be 390 nm or shorter which corresponds to ultraviolet (UV) radiation or photons with even higher energies. Although the majority of studies about uranyl photoreduction using anatase have adopted light sources with the primary emission in the UV-A range (315 – 400 nm), some medium-pressure mercury lamps do not filter contributions of radiations having shorter and longer wavelengths (Salomone and others, 2015). More electrons would overcome the bandgap of semiconductors as the wavelength of UV radiation is shorter. It is questionable whether UV radiation with shorter wavelengths and thus more electron-hole pairs in the anatase catalyst will be either cooperative or inhibitive to uranyl photoreduction. Indeed, selection among different UV types is one of the most important parameters in optimizing photochemical treatments of organic and inorganic contaminants as well (Alaton and others, 2002).

The main objective of this study is to investigate 1) the respective role of organic molecules on complexation and electron donation during heterogeneous photoreduction of uranyl and 2) the dependence of the uranyl photoreduction with various organic molecules on UV wavelength. Four different organic ligands were selected as electron donors: acetate, EDTA, oxalate, and hydroquinone. There are previous studies that used acetate and EDTA as an electron donor for uranyl reduction (Chen and others, 1999; Bonato and others, 2008). To our knowledge, the present study is the first to demonstrate the oxidation of oxalate and hydroquinone as coupled with photocatalytic uranyl reduction. The three subclass regions of the UV spectrum, UV-A, B, and C, are used to examine how uranyl photoreaction with varying organic ligands responds to these regions of UV light. X-ray photoelectron spectroscopy (XPS) was adopted to obtain direct evidence for U photoreduction as catalyzed by TiO_2. Based on the uranium speciation with the organic ligand, reaction mechanisms and effects of organic ligands and UV wavelengths on photocatalytic reduction of uranyl are discussed.

TABLE 1

Summary of solution chemistry and experimental conditions

Solution chemistry			Remarks
$[U]_{ini}$	0.21 mM		U(VI) : Org. is ranged 1:2 to 1:8
[Org.]	0.42 to 1.68 mM		(Org. is acetate, EDTA, oxalate and hydroquinone)
pH	2.5		
$[O_2]$	Solution degassed		< 1 ppm in atmosphere
Temperature	25 °C		
Experimental set	Constraints		Main process in uranyl removal
	Irradiation	with Catalyst	
I.	No	Yes	Adsorption
II.	Yes	No	Homogeneous photoreduction
III.	Yes	Yes	Adsorption + photoreduction

METHODS

Materials and Reagents

Titanium oxide (TiO_2) nanoparticles (AEROXIDE® TiO_2 P25) were provided by Degussa and used without further purification. P25 consists of aggregated primary particles of anatase and rutile, two polymorphs of titanium oxide, in a weight ratio of 4:1. Particle mean diameter is 21 nm and the specific surface area is 50 m^2/g. Prior to solution preparation, Milli-Q® water (resistivity ≥ 18.2 MΩ·cm) was autoclaved in Pyrex® media storage bottles at regular sterilizing conditions (that is, 40 min at 121°C and 138 kPa). Immediately after, purified N_2 was bubbled into the water through a diffuser for about 60 min while the water cooled from 95 to 40 °C. Glass bottles were then capped air-tight and immediately transferred to a controlled-atmosphere glove box. Stock solutions of uranyl and organic compounds were prepared using uranyl nitrate hexahydrate ($UO_2(NO_3)_2{\cdot}6H_2O$, International Bio-analytical Industries), sodium acetate trihydrate ($NaCH_3COOH{\cdot}3H_2O$, Fisher Chemical), disodium EDTA dihydrate ($C_{10}H_{14}N_2Na_2O_8{\cdot}2H_2O$, Fisher Chemical), oxalic acid dihydrate ($C_2H_2O_4{\cdot}2H_2O$, Baker analyze) and hydroquinone ($C_6H_6O_2$, Acros Organics).

Solution Chemistry and Irradiation Experiments

Experimental settings used in this study are summarized in table 1. For all experiments, the concentration of uranyl was 0.21 mM while the concentrations of organic compounds were varied from 0.42 to 1.68 mM which correspond to the uranyl to organic compound molar ratio of 1:2 to 1:8. Control experiments were run without titanium oxide catalyst or in darkness (set I and II in table 1) to explore synergistic effects in the coexistence of the catalyst with the light source (set III). The solutions were initially adjusted to a pH of 2.5 by adding concentrated NaOH or HCl. This value of pH was selected because only a minimal change in pH (< 0.2) occurs after 5 h of the photoreaction in solutions used in this study. After the reaction, the solution was filtered, and the supernatants were collected and analyzed by a Perkin-Elmer ELAN DRC-e inductively coupled plasma mass spectroscopy (ICP-MS). In this study, dissolved uranium measured after the reaction corresponds to the uranyl remaining in solution after adsorption to the solid phase and precipitation as uranium-containing solids.

For our experimental conditions, aqueous U(VI) species and saturation index with respect to various solid phases were calculated by Visual MINTEQ ver. 3.0 with the Thermo.vdb database (fig. 1). Speciation of uranyl is variable depending on the

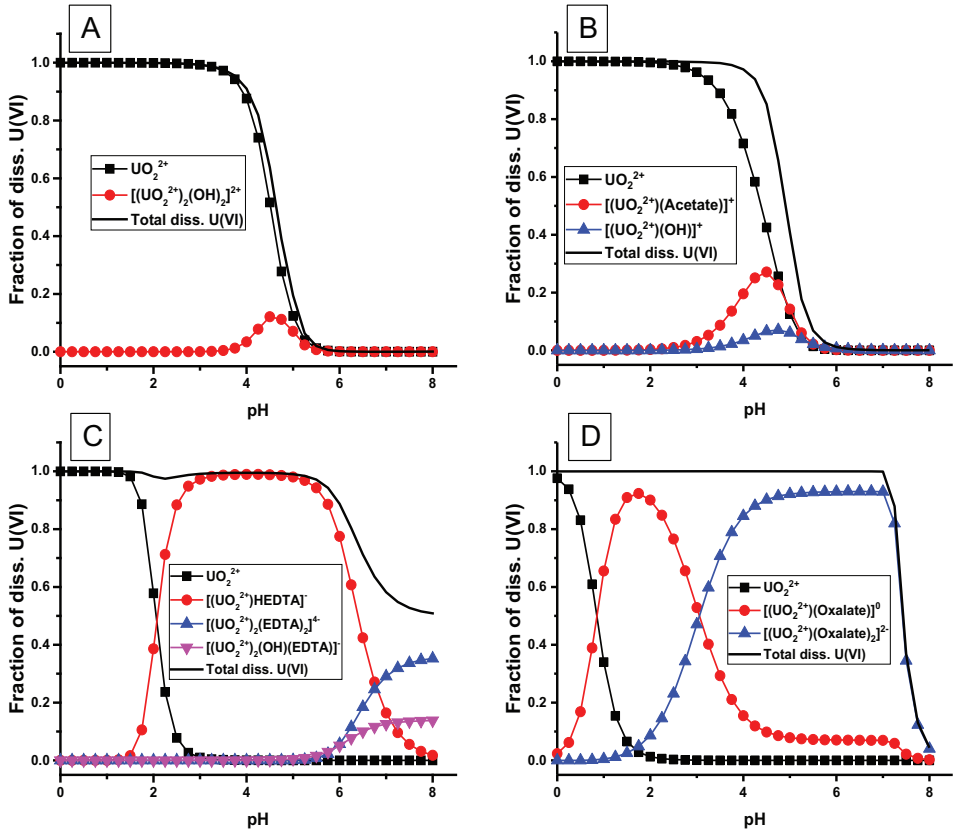

Fig. 1. Speciation of dissolved uranyl (A) as a function of pH (0.21 mM U(VI)), (B) in the presence of 1.68 mM acetate, (C) 1.68 mM EDTA, and (D) 1.68 mM oxalate. Decrease in the total dissolved U(VI) at pH 6 to 10 is mainly due to precipitation of schoepite and U-hydroxides.

dissolved organic ligand and its concentration. Experiments in acidic solutions (pH 2.5 in this study) are valid for our experimental purpose as the possibility of wet precipitation of uranyl solids can be ruled out at such a low pH (fig. 1).

Photocatalytic experiments with TiO_2 suspensions were carried out using an in-house fabricated photoreactor consisting of three vessels nestled inside one another (fig. 2). The quartz inner vessel is a thimble designed to hold a compact fluorescent bulb (Philips 9 W, G23). This inner vessel is positioned inside a central reaction vessel, which in turn sits inside an outer vessel. The outer vessel holds a thermostatic layer of circulating water controlled by an external water chiller. UV light bulbs providing different wavelength ranges were used: (1) 368 nm emission peak for the UV-A region, (2) 311 nm emission peak for the UV-B region, and (3) 254 nm emission peak for the UV-C region. TiO_2 suspensions (65 mL, $1gL^{-1}$) were irradiated in an anoxic glovebox (< 1 ppm O_2) with a 10 percent H in N gas mix.

Material Characterization

XPS spectra were collected using an Axis Ultra spectrometer (Kratos Analytical UK). Monochromatic and focused Al K^{α} radiation (1486.6 eV) was used for the excitation of samples. All measurements were performed in the hybrid mode, which

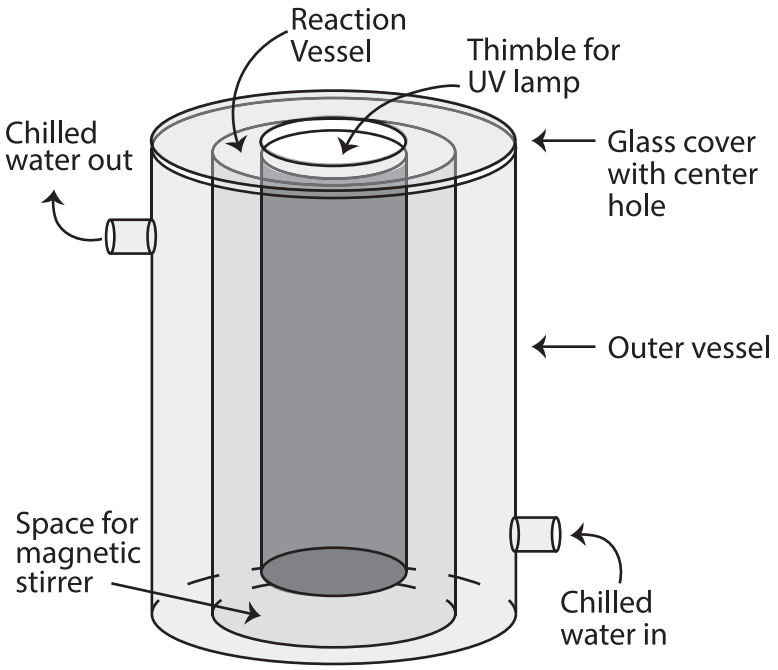

Fig. 2. Illustration of the photoreaction apparatus used in this research. The elongated UV lamp is housed inside the inner quartz thimble in direct contact with the solution to induce photoreactions. Dissolved oxygen can compete with U(VI) for electrons transferred from an electron donor species. To minimize the effect of oxygen, the apparatus is set up in a glove box to maintain anoxic conditions; all solutions are prepared with degassed water. A water chiller outside the glove box is connected to the reaction vessel inside to keep temperature constant during the course of experiments.

employs both electrostatic and magnetic lenses. The x-ray emission current and anode voltage used during spectra acquisition were 8 mA and 14 keV, respectively. Survey and core scans were acquired at constant pass energies of 160 and 20 eV, respectively. Measurements were performed under vacuum conditions lower than 10^{-8} Torr. All spectra reported were calibrated using the position of the Ti 2p peak (458.7 eV) or the C 1s peak (284.9 eV) for adventitious carbon. Spectra analysis and calibration were performed using the CASA XPS software (version 2.3.16, www.casaxps.com). Caution is needed on XPS analysis for uranium because U(VI) is likely reduced during exposure to the X-ray beam (Ilton and others, 2007). Sequential analyses were taken on the same spot, for each specimen, in order to check for beam-induced reduction as suggested by Ulrich and others (2009). The specimen with EDTA was stable over the first several spectra whereas oxidation state measurements of the specimens with acetate and the uranyl adsorption sample suggested reduction over time. Fortunately, reduction was found to be systematic and slow. The XPS spectra presented in this work are always the first two scans in each measurement such that the contribution of the beam-induced reduction to the XPS spectra is minimal.

Microscopic morphologies of solid phases before and after the catalytic photoreaction were examined using scanning electron microscopy (SEM, Hitachi, S-4800) equipped with an EDX spectrometer.

Modeling Molecular Structures of Uranyl-Organic Complexes

Energy optimizations of uranyl-organic complexes were performed using the software package DMol^3 (Local Density Functional Calculations on Molecules) (Delley,

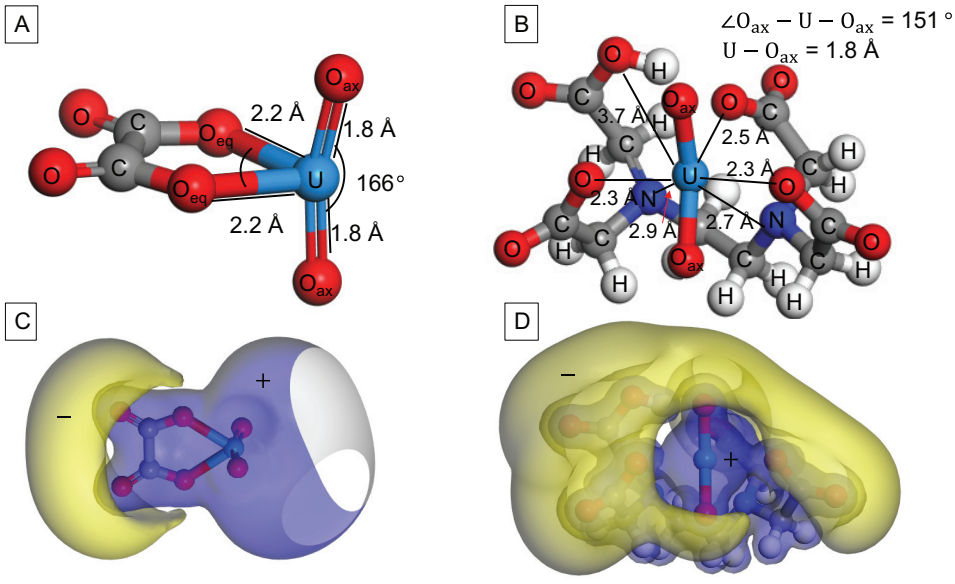

Fig. 3. Energy-optimized structures and electrostatic potential surfaces of $[(UO_2^{2+})(oxalate)]^0$ (A, B) and $[(UO_2^{2+})HEDTA]^-$ (B and D). In figures 3C and 3D, the blue and yellow surfaces represent positive and negative potentials, respectively.

1990). The Perdew-Wang generalized gradient scheme (GGA) was used in combination with ultrasoft pseudopotentials. The GGA scheme was parameterized by the Perdew-Burke-Ernzerhof (PBE) functional (Perdew and others, 1996). The double numeric quality basis set (DNP) and effective core potentials (ECPs) were used for all calculations. The convergence tolerance for energy change, max force, and max displacement were 2×10^{-5} Ha, 0.004 Ha $Å^{-1}$, and 0.005 Å, respectively. A Fermi smearing of 0.01 Ha to the orbital occupancy was applied to improve computational performance.

The uranyl species of $[(UO_2^{2+})(C_2O_4)]^0$ and $[(UO_2^{2+})HEDTA]^-$ were modeled and their energy-optimized structures are shown in figures 3A and 3B. The initial model of $[(UO_2^{2+})(C_2O_4)]^0$ before optimization was adopted from Tsushima and others (2010). To our knowledge, there have been no studies reporting the coordination environment of uranyl forming a complex with EDTA. The $EDTA^{4-}$ anion has 4 O atoms belonging to the carboxyl functional group and two N atoms that can form bonds with the central cation during chelation. When modeling chelation with EDTA, having uranyl as a center metal ion is not simple because it has two O atoms that may induce some steric restrictions. Several possible configurations of $[(UO_2^{2+})HEDTA]^-$ were built while considering some important parameters such as H bonding with N and O, and coordination number of UO_2^{2+} from 4 to 6 with the N and O atoms of EDTA. From energy optimization of those configurations tested, the one with the lowest energy is presented in figure 3B.

RESULTS

Speciation and Adsorption of Uranyl in the Presence of Organic Ligands

Speciation of uranyl in the presence and absence of organic ligands is calculated as a function of pH and presented in figure 1. In the absence of organic ligands, the

TABLE 2

Uranyl removal from solution after reaction in darkness and without TiO_2

	U(VI) adsorption by TiO_2 (%)	U(VI) removal without TiO_2 (%)		
UV Light	dark	368 nm	311 nm	254 nm
Acetate	9.0	8.9	5.1	3.8
EDTA	10.2	0.0	4.0	1.7
Oxalate	1.3	11.9	12.2	6.1
HydroQ	5.8	8.7	7.3	0.8

UO_2^{2+} ion is the most dominant uranyl species in acidic solutions (pH $<$ 4.0, fig. 1A). The total U(VI) concentration of 0.21 mM decreases at pH values above 4.0 due to the formation of uranyl oxyhydroxide solids such as schoepite. In the presence of an organic ligand, uranyl tends to remain in solution and the total dissolved U concentration remains constant over a wider range of pH. Among acetate, EDTA, and oxalate, acetate shows the weakest binding with the UO_2^{2+} ion such that the fraction of the uranyl-acetate complex is calculated to be less than 30 percent in acidic conditions (fig. 1B). The formation of uranyl-ligand complexes plays a critical role in solution chemistry of uranyl with EDTA and oxalate. The fraction of the UO_2^{2+} ion drastically decreases with increasing pH, and the uranyl-ligand complex is the most dominant species at pH above 2.0. $[(UO_2^{2+})HEDTA]^-$ is the dominant uranyl species in the presence of EDTA, while $[(UO_2^{2+})(C_2O_4)]^0$ and $[(UO_2^{2+})(C_2O_4)_2]^{2-}$ are major species in oxalate solutions at pH 2.5 (figs. 1C and 1D).

Uranyl removal from solution in the absence of UV radiation is due to adsorption on TiO_2 (table 1). Uranium uptake by TiO_2 is the highest in uranyl solutions with EDTA (10 %) and acetate (9 %), followed by hydroquinone and oxalate (less than 6 %) (table 2). Adsorption of uranyl on TiO_2 is largely controlled by the surface charge of the adsorbent (Cerrillos and Ollis, 1998). The point of zero charge of P25 TiO_2 nanoparticles is near pH 4 to 5 (Noh and Schwarz, 1989). This means that the surface of the TiO_2 particles is positively charged at pH 2.5 and thus repulsive to the UO_2^{2+} ion. Such electrostatic interactions between the surface and the adsorbate can be influenced by the organic ligand. The organic ligand can be adsorbed onto the catalyst thereby reducing the solid surface excess positive charge. Additionally, the charge of the uranyl species can be modified by complexation with the organic ligand, and the resulting uranyl-ligand complexes may be preferentially partitioned into either the solution or the solid phase. For example, the lowest adsorption of uranyl onto TiO_2 is found from solution with oxalate. At pH 2.5, the dominant oxalate species dissolved in solution is monobasic oxalate ($HC_2O_4^-$). The monobasic oxalate anion may have a strong affinity toward the TiO_2 surface and counterbalance the positive charge of the proton-dominated TiO_2 surface site with its negative charge. Such a mechanism would lessen the interaction of the negatively charged species, $[(UO_2^{2+})(C_2O_4)_2]^{2-}$, with the TiO_2 surface. Although $[(UO_2^{2+})(C_2O_4)]^0$ is dominant in solution with oxalate, it might be moderately or least reactive toward the TiO_2 surface due to its neutral charge.

Although metal-organic molecules are present in hydrated forms in solution, the water ligands would be the first to be desorbed because they are more weakly bound than the organic ligand. Thus, the proportion of dehydrated species would increase toward the surface region where they interact with reactive surfaces of the solid phase and form bonds with the surface functional group. This tendency has been shown for

uranium interacting with the TiO_2 surface where uranium of the uranyl molecule forms bonding directly with oxygen on the surface, for example, in the bidentate mode [Perron and others, 2006, see also the excellent review regarding the structures of hydrated uranyl complexes (Kubicki and others, 2009)]. Here, the molecular structures of uranyl species, $[(UO_2^{2+})(C_2O_4)]^0$ and $[(UO_2^{2+})HEDTA]^-$, were calculated to consider the reactivity of these molecules upon interaction with the catalyst surface. When a uranyl ion forms a complex with an oxalate anion, the two O atoms of uranyl (axial oxygen in fig. 3A) are bent and form an O-U-O angle of 166°. The two O atoms of oxalate are equatorially positioned with respect to the uranyl structure (equatorial oxygen in fig. 3A). The structure of the uranyl molecule shows the $U\text{-}O_{ax}$ distance of 1.8 Å and the $U\text{-}O_{eq}$ distance of 2.2 Å. These U-O bond distances are approximately the same as previous reports of uranyl-oxalate complexes (Tsushima and others, 2010). In the model of $[(UO_2^{2+})HEDTA]^-$, the angle between the U atom and the axial O atoms are 151° and their distance is 1.8 Å (fig. 3B). The uranyl forms five-fold coordination with three O atoms of the carboxyl functional group and two N atoms and the U-O distance is 2.3 to 2.5 Å and the U-N distance are 2.7 and 2.9 Å. The oxygen bonded with H is farther away from the uranium atom (3.7 Å). The distances between central uranium and the five nearest N and O atoms are close to values reported from previous studies of uranyl-formate complexes (Lucks and others, 2013).

The electrostatic potential of individual complexes are presented in figures 3C and 3D. The negative potential is mainly distributed near the two nonbonding O atoms of $[(UO_2^{2+})(C_2O_4)]^0$ while O atoms that belong to the carboxyl functional group of EDTA are the main location of the negative potential in the molecular structure of $[(UO_2^{2+})HEDTA]^-$. Uranyl accounts for the largest portion of positive potential found in the molecules of these uranyl complexes. Since the surface of the TiO_2 catalyst is proton-dominant at pH 2.5, the electron-rich regions of these molecules where the negative potential is dominant would be reactive to interact with the positively charged surface. It is followed that these uranyl-organic molecules are likely bound to the surface through the ligand when adsorbed. This inference is in good agreement with a previous study suggesting that the S-L-M binding mode where the ligand (L) is located between the surface (S) and the metal ion (M) could explain adsorption behavior of uranyl in the presence of EDTA (Cerrillos and Ollis, 1998). In turn, it is supposed that the interaction between uranyl and the catalysts surface can be largely modified by the presence of the organic ligand.

Macroscopic Evidence of Photocatalytic Uranyl Reduction

Dissolved uranyl can undergo several processes in the presence of UV light and TiO_2 catalyst.

[1] The surface of TiO_2 provides reactive sites where the uranyl molecule can be adsorbed (adsorption).

[2] Uranyl may be reduced by interaction with UV light. The process does not involve catalysis by TiO_2, but possibly the oxidation of a coexisting organic compound (homogeneous photoreduction).

[3] Electrons excited by UV light into the conduction band are transferred to the adsorbed uranyl molecule. This process is coupled with the oxidation of an organic compound that acts as a hole-scavenger (heterogeneous photoreduction).

Experimental sets to estimate the contributions of individual processes are summarized in table 1 and experimental results are presented in table 2 and figure 4.

At pH 2.5, uranyl removal by TiO_2 without UV light (that is, adsorption) is $\leq$10 percent in the presence of acetate, oxalate, hydroquinone or EDTA (table 2). Uranyl removal by photoreaction without TiO_2 particles (that is, homogeneous photoreduction) is less than 10 percent for solutions containing acetate, EDTA and hydroquinone,

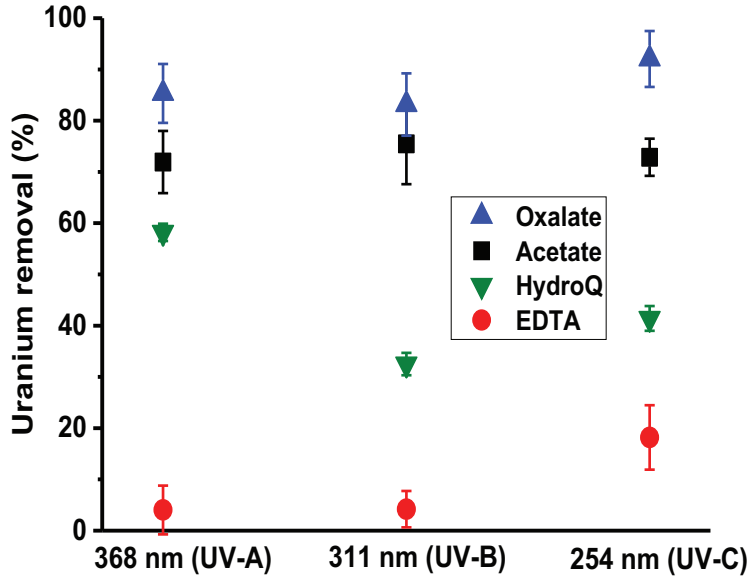

Fig. 4. Uranium removal from solutions containing different organic compounds. $[U(VI)]_{ini}$ = 0.21 mM, $[Org.]_{ini}$ = 1.68 mM, pH = 2.5 and 1 g/L of TiO_2. The error bars represent data from replicate experiments.

and 6 to 12 percent for solution with oxalate depending on the UV region (table 2). Assuming these two processes were always independent, their maximum contribution would be ≤~22 percent for all possible combinations of organic compound and UV light region. Figure 4 shows the effect of different UV light wavelengths on uranyl removal from organic compounds solutions in the presence of TiO_2. For solutions containing acetate, oxalate, and hydroquinone, photolytic uranyl removal by TiO_2 is more than 30 percent over all UV regions, 2/3 or more of which can be associated to the influence of the UV source and/or the TiO_2 catalyst.

Among organic molecules tested in this study, the most effective electron donors are acetate and oxalate which show uranium removal of more than 70 percent for all the UV lights tested, followed by hydroquinone and EDTA (fig. 4). There are no significant differences in uranyl removal between the three UV regions when acetate and oxalate are present in solution as an electron donor. Uranyl removal depends highly on the UV light range when uranyl coexists with EDTA and hydroquinone, but dependence on UV wavelength is found contrasting between the latter two compounds. Uranyl removal is the greatest in the UV-A region for solutions containing uranyl and hydroquinone, whereas maximum removal of uranyl from solutions with EDTA occurs in the UV-C region.

Since the organic compounds show different efficiencies as electron donors for uranyl removal (that is, oxalate > acetate > hydroquinone > EDTA), it is worth testing whether the efficiencies of hydroquinone and EDTA are enhanced by adding acetate (or oxalate). The coexistence of acetate and hydroquinone increases uranyl removal by ~15 percent whereas uranyl removal with EDTA marginally changes when the same concentration of acetate is added to the solution (fig. 5A). However, decreasing EDTA concentrations enhances uranyl photoreduction by TiO_2 (fig. 5B). Uranyl removal increases as the uranyl to EDTA molar ratio increases from 1:8, to 1:4, and to 1:2. This observation suggests that dissolved EDTA species can act as electron donors but hinder the uranyl removal as its concentration reaches certain levels.

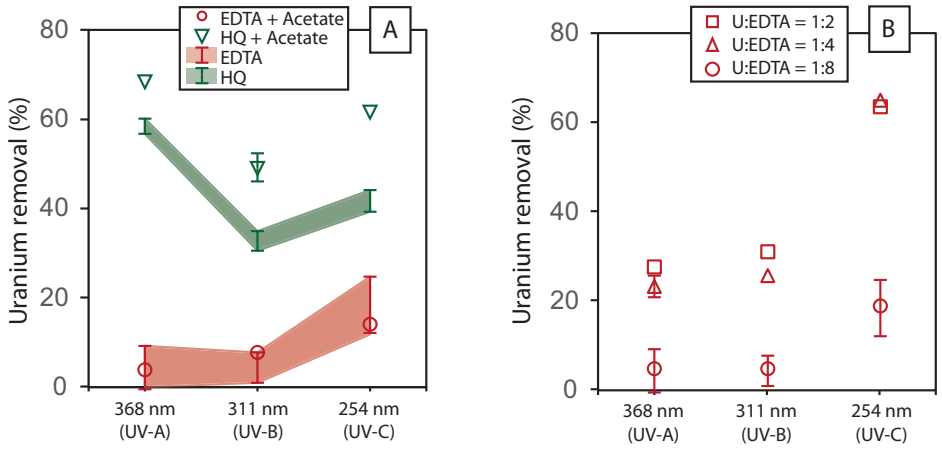

Fig. 5. (A) Effects of adding 1.68 mM acetate on uranium removal from different solutions. Red symbols: 0.21 mM of U(VI) and 1.68 mM of EDTA. Green symbols: hydroquinone. (B) Uranyl removal from solution ($[U(VI)]_{ini}$ = 0.21 mM) with varying concentrations of EDTA (0.42 mM, 0.84 mM, and 1.68 mM). The colored rectangles on fig. 5A are error bars from replicates. The absence of bars indicate the error is smaller than the symbols.

These results of uranium solution chemistry show that mechanisms of uranyl photocatalytic reduction can vary depending on the coexisting organic molecule functioning as a ligand and an electron donor. Specific effects of organic ligands are discussed further in the discussion section.

Forms of Uranium after Photoreaction with Organics

XPS analysis is performed to measure variation in the oxidation state of uranium as a result of the photoreaction. The binding energies of uranium are analyzed to identify possible forms of uranium in the reacted solid phase such as uranium oxides and uranium-organic complexes.

XPS core scans of the U 4f peaks are presented in figure 6. Uranyl nitrate hexahydrate was used as reference material and shows two peaks centered at 382.8 and 393.6 eV, which corresponds to U4f 7/2 and 5/2 spin-orbit split peaks, respectively (data are not shown here). These binding energies are comparable to other reported values of U(VI) in uranyl nitrate hexahydrate (Dash and others, 1999; Froideval and others, 2003). In samples from photoreactions with acetate and EDTA, the U 4f peaks are shifted to lower binding energy by ~2.4 eV (figs. 6A and 6B), which is likely indicative of the presence of uranium species with the oxidation states of U(V) and U(IV).

Distinguishing among the different oxidation states of uranium (IV, V and VI) is not straightforward in samples with mixed oxidation states because the primary peaks lie within 3 to 4 eV. Notwithstanding, satellite structures that are observed around the primary peaks can be used to assist in identification of peaks. Specifically, the U(VI) species typically display satellites at around 4 and 10 eV above the primary spin orbit split U4f peaks while satellites that belong to U(IV) and U(V) species tend to appear at ~6 and ~8 eV above, respectively. Based on such a relationship between the primary peak and the satellite, we fit three components to the main peaks and satellites of the XPS spectra of uranyl photoreaction with acetate and EDTA to discern uranium species with different oxidation states (fig. 6). The fitting procedure documented by Ilton and Bagus (2011) is followed in this study. Fitting was performed with characteristic fit parameters being constant, such as the shapes and full width at half maximum

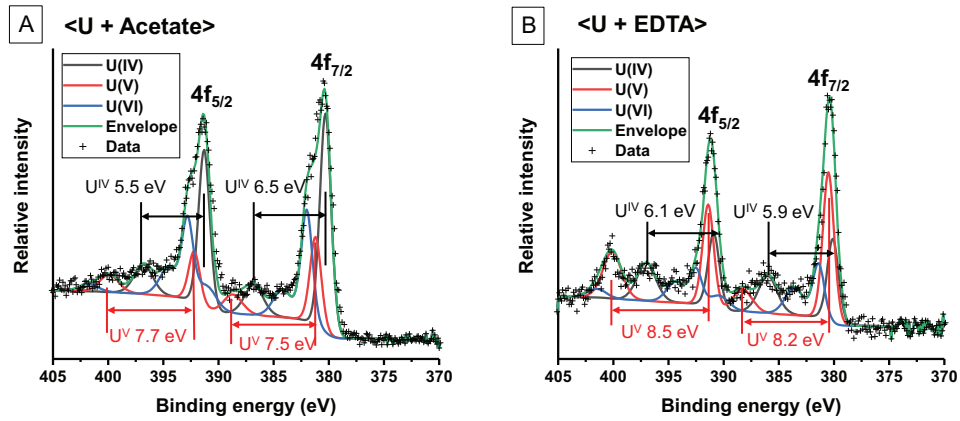

Fig. 6. The fits to the core scans of U 4f orbitals (A) for uranyl photoreduction with acetate (pH 2.5; $[U]_{ini}$ = 0.21 mM and $[acetate]_{ini}$ = 1.68 mM; 5 h radiation with UV-A) (B) with EDTA (pH 2.5; $[U]_{ini}$ = 0.21 mM and $[EDTA]_{ini}$ = 0.84 mM; 5 h radiation with UV-A).

(FWHM) of the primary peaks; in addition, the relative ratio of FWHM of the satellite to that of the main peak are identical among peak components with different oxidation states (Ilton and Bagus, 2011). Peak separations between the primary and satellite peaks are found to be 6.0 ± 0.4 and 8.0 ± 0.5 eV, for U(IV) and U(V), respectively (fig. 6). The fit data confirm that U(IV) and U(V) species result from the uranyl photoreaction with acetate and EDTA. The proportions of U oxidation states were (50%/20%/30% for U(IV)/U(V)/U(VI)) from the acetate solution and (33%/47%/20% for U(IV)/U(V)/U(VI)) from the EDTA one (table 3). In other words, in the acetate-containing sample, 70 percent of U had been reduced by one or two electrons and in the EDTA-containing one, that fraction was 80 percent (table 3). The dominant uranium oxidation state is U(IV) in the sample with acetate (50 % in atomic proportion) and U(V) in the sample with EDTA (47 %). The primary peak positions of

TABLE 3

XPS primary peak positions and atomic proportions of uranium oxidation states

U + acetate			
	U(IV)	U(V)	U(VI)
$U4f_{7/2}$	380.3	381.2	382
$U4f_{5/2}$	391.3	392.2	392.8
Atomic proportion	0.50	0.20	0.30
U + EDTA			
	U(IV)	U(V)	U(VI)
$U4f_{7/2}$	380.1	380.5	381.4
$U4f_{5/2}$	390.9	391.4	392.5
Atomic proportion	0.33	0.47	0.20

$U4f_{5/2}$ and $U4f_{7/2}$ for each oxidation state are lowered consistently by 0.2 to 0.8 eV in the sample with EDTA than the one with acetate. These U XPS results suggest that reaction products are not identical between photoreactions with acetate and EDTA.

Previous studies suggest that redox transformation of U(VI) to U(IV) is the dominant process of uranyl photoreduction as catalyzed by TiO_2 and that U(IV) oxides such as UO_2 and UO_{2+x} ($x = 0$ to 0.25) are the primary product of the process (Chen and others, 1999; Kim and others, 2015; Salomone and others, 2015). This general conclusion would be the case when the UO_2^{2+} ion is the main reactant to be subject to reduction during the catalytic photoreaction. In solution of pH 2.5 with acetate, the dominant uranium species is the UO_2^{2+} ion (fig. 1B) and U(IV) species detected in the XPS spectrum is attributed to U(IV) oxides. From SEM measurements, microscopic morphologies of the solid phases are similar before and after the photocatalytic reaction with acetate (fig. 7). The EDS mapping results show a uniform distribution of uranium in micrometer scales (data not shown here). It is inferred that U(IV) oxides would be in the form of precipitates on the TiO_2 nanoparticle in smaller sizes than the substrate. This inference is consistent with a previous study which reports uniform distributions of uranium precipitates in sub to few nanometer sizes on TiO_2 electrodes after photochemical and electrochemical reduction (Kim and others, 2015). U(V) dominates over U(IV) in the sample reacted with EDTA (table 3). The presence of U(IV) could be partially attributed to U(IV) oxide precipitates as similar to photoreaction with acetate. It has been considered that UO_2^{+} is not as stable as UO_2^{2+} and $UO_{2(s)}$ and undergoes a disproportionation reaction to form the latter species (Renock and others, 2013; Yuan and others, 2015). In solution with EDTA, however, U(VI)-EDTA complexes are dominant over the UO_2^{2+} ion at pH 2.5 (fig. 1C) and can be reduced to U(V)-EDTA and possibly U(IV)-EDTA without decomplexation (Baker and Sawyer, 1970; Chen and others, 1999). This explanation is also consistent with the XPS results showing lower binding energies of uranium species from photoreaction with EDTA than those with acetate.

DISCUSSION

Mechanisms of Photoreduction of Uranyl and Uranyl-Organic Complexes Catalyzed by TiO_2

Our experiments demonstrate the dependency of the uranyl photoreduction with varying organic ligands on the energy of UV light. Uranyl photoreduction mediated by the TiO_2 catalyst proceeds through three sequential steps: (i) the formation of the electron-hole pair by photons; (ii) electron transfer into uranyl species; and (iii) oxidation of organic compound to scavenge the hole. In this section, these individual steps of uranyl photoreduction are examined and reaction mechanisms in relation to complexation with organic ligands and photoexcitation by UV lights are specified.

In our experimental setting, the formation of the electron-hole pair takes place when electrons in the valence band gain energies greater than the band gap of TiO_2 as radiated with UV light. The energy gap between the valence and conduction bands in TiO_2 is 3.2 eV and can be overcome by all UV light regions used in this study as calculated from the energy associated with radiation:

$$E = h\nu \tag{1}$$

where h is the Plank's constant ($6.626 \cdot 10^{-34}\,J \cdot s$) and ν is the frequency of light (s^{-1}). UV light with shorter wavelengths provides photons with higher energies. This means that some proportion of excited electrons occupy higher energy states in the conduction band that are not available from photoexcitation with longer UV wavelengths (the energy diagram in fig. 8). Whether uranyl species can gain electrons from the conduction band is determined by their relative energies: Electrons are transferred between those energetic states in the conduction band and the electron acceptor,

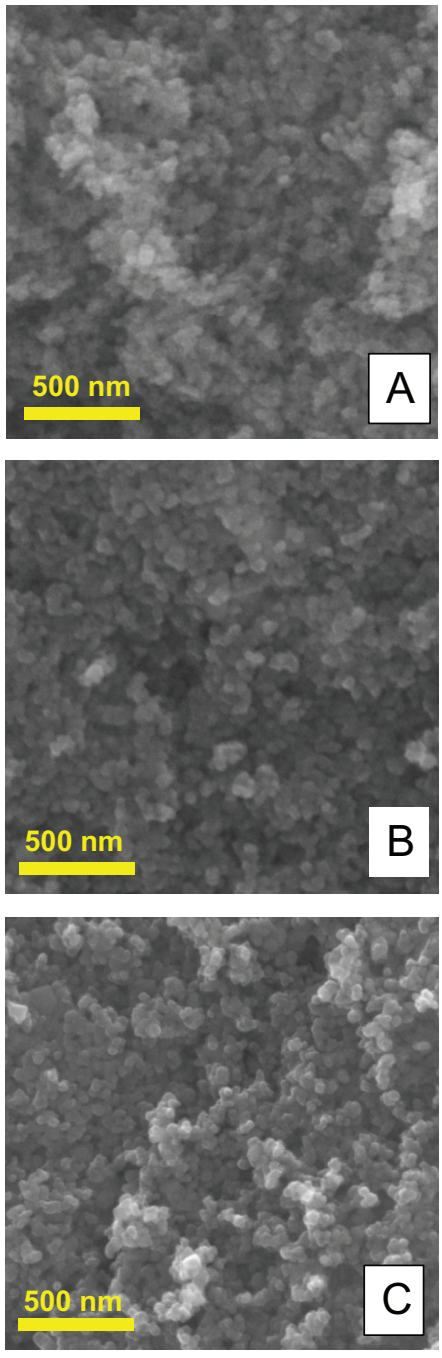

Fig. 7. SEM images of P25 TiO_2 particles. (A) Unreacted samples, and (B) photoreacted samples in solution containing uranyl and acetate and (C) in solution containing uranyl and EDTA.

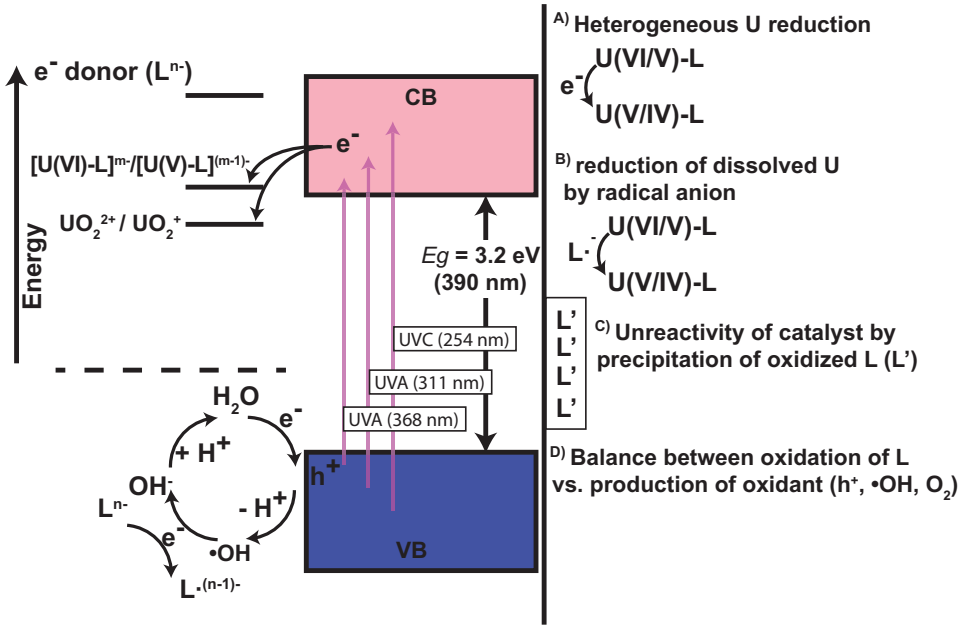

Fig. 8. Simplified energy diagram of the photocatalytic uranyl reduction in the presence of organic electron donors and proposed processes involving organic ligands that can influence the uranyl photoreduction. The results of this study suggest that uranium photoreduction can be mediated by not only (A) mineral catalyst but also (B) radical anions such as $CO_2^{\bullet-}$. (C) Precipitation of oxidation products of electron donating organics can hinder further photoreduction of uranyl. (D) Oxidation of organic ligands is essential to promote uranium reduction and it is balanced with production of oxidants matters with varying the UV wavelength to prevent the reoxidation of reduced uranium species.

which are at approximately the same energy level (Xu and Schoonen, 2000). The standard electrode potential of reaction between UO_2^{2+} and UO_2^{+} is 0.163 V, and the standard electrode potential of the uranyl-organic complexes are lower than this value due to the electron-donating ability of organic ligands (Morris, 2002; Kim and others, 2009). In other words, the energy level of the uranyl-organic complex is higher than that of the uranyl ion such that electrons must be excited to higher energetic states in the conduction band to be transferred to the uranyl-organic complex (the energy diagram in fig. 8). This justification accounts for the trend of uranyl photoreduction with EDTA where uranyl removal is greater by a factor of two or three when photons are sourced from UV-C light than UV-A and B (fig. 5B). It is found that the uranyl removal with acetate and oxalate is nearly constant with varying the UV wavelength (fig. 4). Because the uranyl ion is the dominant species in solution with acetate, it is inferred that photons in the UV-A, B and C regions have sufficient energies to excite electrons to energetic states in the conduction band that coincide with the energy level of the uranyl ion. If only the photo flux and energy are the main limiting factor during the uranyl photo reaction, the photoreaction with an organic compound would be the highest at the UV-C region or nearly constant over all UV regions. However, the photoreaction with hydroquinone is lower in the UV-B and UV-C compared to the UV-A region. This observation indicates that there are limiting factors other than the photon flux and energy that influence the uranyl photoreduction with organic compounds. This peculiar trend of the photoreaction with hydroquinone is discussed further in the following section.

After the electron-hole pair is formed by photoexcitation, electrons are transferred to adsorbed uranyl species (eq 2) and the hole (h^+) serves as a mediator to couple uranyl reduction with oxidation of other species (fig. 8). One such coupled reaction would be water oxidation by the hole (h^+) in the valence band to obtain an OH radical (·OH) (eq 3).

$$U(VI/V) + e_{CB}^- \rightarrow U(V/IV) \quad (2)$$

$$H_2O + h_{vB}^+ \rightarrow \cdot OH + H^+ \quad (3)$$

·OH can undergo self-combination to form hydrogen peroxide (H_2O_2), which in turn produces an oxygen molecule (O_2) as the final product. Although reduced U(V) and U(IV) species are not stable in the presence of h^+, ·OH, or O_2, organic compounds can scavenge those oxidants, and in doing so, promote uranyl reduction. Organic or inorganic radicals can result from the reaction between the organic compound and the oxidants.

Forouzan and others (1996) suggested that oxalate undergoes a two-step process of oxidation with an intermediate radical. The first step is to decompose the molecule into CO_2 and the radical anion ($CO_2^{\cdot -}$) (eq 4). In the second step, $CO_2^{\cdot -}$ donates an electron to the metal ion. This suggestion can be applied to our experiments as stated in equations (4) and (5).

$$HC_2O_4^- + h_{vB}^+ \rightarrow CO_2 + CO_2^{\cdot -} + H^+ \quad (4)$$

$$CO_2^{\cdot -} + U(VI/V) \rightarrow CO_2 + U(V/IV) \quad (5)$$

Acetate and EDTA have carboxyl groups (COOH or COO^-) in the structure and react with either the valence band hole or the OH radical to produce organic radicals (eqs 6 and 7).

$$R\text{-}CH_2COO^- + h_{vB}^+ \rightarrow R\text{-}CH_2COO^{\cdot} \quad (6)$$

$$R\text{-}CH_2COO^- + \cdot OH \rightarrow R\text{-}CH_2COO^{\cdot} + OH^- \quad (7)$$

The organic radicals undergo further reactions possibly involving water and the valence band hole generating CO_2 and oxidation products (for example, eqs 8 and 9).

$$R\text{-}CH_2COO^{\cdot} \rightarrow RCH_2^{\cdot} + CO_2 \quad (8)$$

$$RCH_2^{\cdot} + H_2O + h_{vB}^+ \rightarrow RH + CH_2O + H^+ \quad (9)$$

Hydroquinone is the major product of the photocatalytic phenol oxidation mediated by TiO_2 and its oxidation results in the formation of quinone (Sobczynski and others, 1999). Therefore, the oxidation of hydroquinone to quinone is one likely reaction to be coupled with the photocatalytic reduction of uranium species in solution with hydroquinone.

Effects of Organic Ligands on Uranyl Photoreduction

The present and previous studies (Chen and others, 1999; Madden and others, 1997) propose that uranyl-ligand complexes are photochemically reactive and reduced to form U(V)-ligand complexes as catalyzed by TiO_2 nanoparticles (fig. 8A). EDTA and oxalate form strong complexes with uranyl, such as $[(UO_2^{2+})HEDTA]^-$, $[(UO_2^{2+})(oxalate)]^0$, $[(UO_2^{2+})(oxalate)_2]^{2-}$, and possibly $[(UO_2^{2+})(oxalate)_3]^{4-}$ (see Vallet and others, 2003) and these complexes can be potential species to preserve the oxidation state of U(V) and U(IV) after photochemical reduction of uranyl (fig. 6 and text). Although the role of organic molecules seems manifest on complexation and redox transformation of uranyl during the photochemical process, their oxidation

processes are complicate and are barely known in connection with the uranyl photoreduction. In this section, some of the results are revisited to discuss possible processes that involve organic molecules and influence the uranyl photoreduction.

The process of adsorption is a critical step in the reaction pathway for a reactant to undergo heterogeneous photoreaction. Intriguingly, our data of adsorption and heterogeneous photoreaction in solution with uranyl and the organic ligand show that photocatalytic uranyl removal is not necessarily proportional to uranyl adsorption on the catalyst. For example, adsorption of uranyl on TiO_2 is marginal in the presence of oxalate and no UV radiation. However, for the same suspension, removal of uranyl is maximum under UV radiation. Conversely, the highest adsorption of uranyl is found in solution with EDTA whereas photocatalytic reduction of uranyl is limited in the presence of this organic molecule. These observations indicate that reactions that do not involve the catalyst (that is, homogeneous reactions) may contribute to the uranyl removal. The oxidation of monobasic oxalate ($HC_2O_4^-$) is mediated by the anatase catalyst (eq 4). The resulting radical anion ($CO_2^{\cdot -}$) is released into solution and reacts with dissolved uranium species (eq 5; fig. 8B). As a result, one oxalate molecule ion can release two electrons and reduce uranium species via more than one process (eq 2 and 5), which accounts for its highest ability as an electron donor among the four organic ligands tested in this study.

The oxidation of EDTA in the presence of UV irradiation is a source of electrons for uranyl reduction transferred through the TiO_2 catalyst, but uranium removal from solution tends to decrease at high concentrations of EDTA (fig. 5B). After the electron transfer proceeds, reduced uranium species of U(V) and U(IV) that remain in the form of EDTA complexes can be either released into solution or partitioned onto the catalyst surface (fig. 8A). The release of reduced uranium species into solution would be enhanced with increasing the EDTA concentration. This explanation is also consistent with the XPS data results of photoreduction with EDTA showing the dominance of U(V) over other U species and lower binding energies of reduced species than those produced from the reaction with acetate (fig. 6 and text). Another reason for the decrease in uranyl removal at higher EDTA concentrations may be that products of EDTA oxidation precipitate on the surface of TiO_2 while the photoreaction proceeds, such that the catalysis becomes less effective as the reaction proceeds (fig. 8C). This hypothesis is supported by our macroscopic observation that the TiO_2 catalyst turns dark grey after photoreactions in solution of EDTA with and without dissolved uranyl. The hydrogen molecule (H_2) and ethylenediaminetriacetate (ED3A) can be produced as a result of the photooxidation of acetate and EDTA, respectively, as described in equation (9). ED3A is found to undergo sequential oxidation steps that lead to smaller oxidation products when the reaction system is saturated with the oxygen molecule (Babay and others, 2001). In case of photoreaction with hydroquinone, quinone can be oxidized further into other intermediates and ultimately CO_2 and H_2O as long as an oxygen supply is not limited during the reaction (Sobczynski and others, 1999). In our experimental settings, however, gaseous oxygen is limited to less than 1 ppm and dissolved oxygen is removed by water boiling above 100 °C and sequential degassing by N gas (see the methods section). As a result, the oxidation of large organic ligands would not be complete. Such oxidation products could impede further reduction of uranium species mediated by the catalyst.

One peculiar trend observed from the reaction with hydroquinone is that heterogeneous uranyl reduction is lower in the UV-B and UV-C compared to the UV-A region (fig. 4). The heterogeneous photoreduction depends on the production of the electron-hole pair in the catalyst. The production rate of the electron-hole pair increases with increasing UV light energy (fig. 8). With shorter wavelengths of UV light, not only the process of electron transfer to uranyl species but also the reactions

associated with the valence band holes, including the oxidation of organic ligands and the production of strong oxidants, will proceed to a greater extent (eq 3, 4 and 6; fig. 8D). If the oxidation rate of organic ligands is high enough to scavenge the oxidants produced from the valence band hole, oxidation of reduced uranium can be prevented. In the case where the rate of oxidant production is greater than the rate of electron donation from the organic molecule, however, uranyl reduction is hindered, and reduced uranium species are oxidized by the oxidant. It is possible that limited uranium reduction occurs in the UV-B and -C ranges because the production of oxidant surpasses electron donation from hydroquinone to a larger degree than it does in the UV-A range.

Additional experiments on uranyl removal in the absence of organic ligands show that uranyl removal with TiO_2 is not significant ($< 5\%$) at pH 2.5 under no UV light, but after 5 hours of irradiation, increases to levels on the order of uranyl removal with EDTA. Salomone and others (2015) performed uranyl photoreaction experiments in the presence of propanol. They also observed a certain amount of uranyl being removed from solution in the absence of propanol. The removal rates without organic ligands under UV light are a few times lower than the removal rates with oxalate and acetate, which suggest a limited influence at the time-scale of our experiments. Unlike uranyl removal with EDTA, photoreaction without organic ligands produced no gray precipitates under the UV light. This observation suggests that uranyl removal processes differ between solutions with and without organic compounds, and that organic compounds are the primary electron donors to uranyl during the photoreaction with high ratios of organic compound to uranyl as it is suggested in previous related works (Chen and others, 1999; Evans and others, 2004; Bonato and others, 2008; Salomone and others, 2015).

It was beyond the scope of our study to address the processes responsible for uranyl removal by irradiated TiO_2 without organic compounds. These mechanisms remain chiefly unidentified and their contribution cannot be completely ruled out from our experimental setting wherein the photodecomposition of dissolved organic ligands is the major contribution to uranyl removal from solution. Future research should include specific mechanisms of uranyl removal in the absence of organic electron donors.

CONCLUSIONS

This study describes the synergistic interplay between organic ligands (that can provide electrons but also may hinder electron transfer), a catalytic surface, and light in the reduction of uranyl molecules. To our knowledge, the present study is the first to report the dependency of the uranyl photoreduction on the wavelength (or energy) of UV light. Such dependencies are variable depending on organic compounds. Acetate is a good electron donor but does not act as a ligand in our experiments because of its weak binding affinity with uranyl. It has been shown that uranyl photoreduction as coupled with oxidation of acetate is nearly independent of UV wavelength. Oxalate is a good electron donor as well as a strong ligand. Uranyl photoreduction with oxalate is strikingly efficient but may result from multiple processes that can be activated by any photons in the UV-A, B, and C spectrum. Electrons in higher energetic states of the conduction band are required to reduce uranyl-EDTA complexes. The production of such electrons can be further promoted by using UV light with shorter wavelengths. Although EDTA acts as an electron donor, increasing EDTA concentrations does not necessarily assist in enhancing uranyl removal from solution. This is probably because solubility of reduced uranium species increases if they form complexes with EDTA. Hydroquinone is found to act as an electron donor, but its electron donation becomes inefficient to leave uranium in reduced forms as the photon energy increases. This result supports the idea that reduced uranium from photoreduction is preserved only

when the oxidation of organic molecules proceeds at fast rates to overcome oxidant attacks.

The computational results in this study reveal a significant change in the reactivity of uranyl toward the positively/negatively charged surfaces due to the formation of complexes with organic ligands. Further simulations using DFT calculations are necessary to decipher the exact mechanism of surface adsorption and the process of electron transfer within uranyl-organic complexes upon interaction with TiO_2. One could potentially adopt time-dependent DFT calculations to simulate the reduction of a uranyl-organic complex during the course of electron injection from the valence band to the conduction band by UV light (for example, Elenewski and others, 2016).

U(V) remains stable upon the photocatalytic reduction with EDTA whereas U(IV) is the dominant species as a result of photoreaction with acetate. Distinct features in uranium redox chemistry between different electron donors are likely the result of the formation of complexes of reduced uranium species with organic ligands. Our results show that specific effects of organic molecules and UV radiation ranges should be considered when performing photocatalytic uranyl reduction. Yuan and others (2015) demonstrates that U(V) is more stable and stay on the surface longer than previously believed when it is produced from uranyl reduction mediated by magnetite. Our spectroscopic data suggest that U(V) can be an important reaction intermediate upon photo-induced redox transformation of uranium, especially when its stability can be enhanced by complexation with organic molecules.

The extraction or immobilization of U(VI) has been primarily addressed in environments where contamination risk is high. Recent events such as the Fukushima Daiichi nuclear accident suggest that it would be advisable to expand our understanding of uranium removal to other settings (Schneider and others, 2017). In the marine photic zone, uranium chemistry is largely affected by the presence of carbonate. Uranyl-carbonate complexes in the form of $[UO_2{\cdot}(CO_3)_n]$ (typically, n is 1 to 3) are dominant at neutral and weak basic pH (Djogic and others, 1986). Future studies could be aimed at investigating photoreaction of uranyl carbonate complexes, for example, in the absence and presence of TiO_2. Those attempts will address the extraction of dissolved uranyl from natural seawater or the recovery of accidently discharged radionuclide uranium.

ACKNOWLEDGMENTS

The authors are grateful for the support from the U.S. Department of Energy's (DOE) Office of Science, Office of Basic Energy Sciences (BES), Chemical Sciences, Geosciences, & Biosciences (CSGB) Division for the topics of Heavy Element Chemistry and Geoscience (grant number DE-FG02-06ER15783). Y.K. acknowledges support from Samsung Scholarship. Y.K. thanks Thomas Yavaraski for educating to perform ICP-MS and Will Bender for collaborating on the SEM measurement. The authors acknowledge financial support from the University of Michigan College of Engineering and technical support from the Michigan Center for Materials Characterization. We thank M. R. Antonio and one anonymous reviewer for their constructive reviews and are grateful for the editorial handling of R. S. Arvidson.

REFERENCES

Alaton, I. A., Balcioglu, I. A., and Bahnemann, D. W., 2002, Advanced oxidation of a reactive dyebath effluent: Comparison of O_3, H_2O_2/UV-C and TiO_2/UV-A processes: Water Research, v. 36, n. 5, p. 1143–1154, https://doi.org/10.1016/S0043-1354(01)00335-9

Babay, P. A., Emilio, C. A., Ferreyra, R. E., Gautier, E. A., Gettar, R. T., and Litter, M. I., 2001, Kinetics and mechanisms of EDTA photocatalytic degradation with TiO_2: Water Science & Technology, v. 44, p. n. 5, p. 179–186, https://doi.org/10.2166/wst.2001.0281

Baker, B. C., and Sawyer, D. T., 1970, Electrochemical studies of the uranium (VI)-ethylenediaminetetraacetic acid complex: Inorganic Chemistry, v. 9, n. 2, p. 197–204, https://doi.org/10.1021/ic50084a001

Bonato, M., Allen, G. G., and Scott, T. B., 2008, Reduction of U (VI) to U (IV) on the surface of TiO_2 anatase nanotubes: IET Micro & Nano Letters, v. 3, n. 2, p. 57–61, https://doi.org/10.1049/mnl:20080007

Campbell, J. A., Stromatt, R. W., Smith, M. R., Bean, R. M., Jones, T. E., and Strachan, D. M., 1994, Organic analysis at the Hanford nuclear site: Analytical Chemistry, v. 66, n. 24, p. 1208A–1215A, https://doi.org/10.1021/ac00096a711

Cerrillos, C., and Ollis, D. F., 1998, Photocatalytic reduction and removal of uranium from a uranium-EDTA solution: Journal of Advanced Oxidation Technologies, v. 3, n. 2, p. 167–173, https://doi.org/10.1515/jaots-1998-0210

Chen, J., Ollis, D. F., Rulkens, W. H., and Bruning, H., 1999, Photocatalyzed deposition and concentration of soluble uranium (VI) from TiO_2 suspensions: Colloids and Surfaces A: Physicochemical and Engineering Aspects, v. 151, n. 1–2, p. 339–349, https://doi.org/10.1016/S0927-7757(98)00506-8

Dash, S., Kamruddin, M., Bera, S., Ajikumar, P. K., Tyagi, A. K., Narasimhan, S. V., and Raj, B., 1999, Temperature programmed decomposition of uranyl nitrate hexahydrate: Journal of Nuclear Materials, v. 264, n. 3, p. 271–282, https://doi.org/10.1016/S0022-3115(98)00495-4

Delley, B., 1990, An all-electron numerical method for solving the local density functional for polyatomic molecules: The Journal of Chemical Physics, v. 92, n. 1, p. 508–517, https://doi.org/10.1063/1.458452

Djogic, R., Sipos, L., and Branica, M., 1986, Characterization of uranium (VI) in seawater 1: Limnology and Oceanography, v. 31, n. 5, p. 1122–1131, https://doi.org/10.4319/lo.1986.31.5.1122

Elenewski, J. E., Cai, J. Y., Jiang, W., and Chen, H., 2016, Functional mode hot electron transfer theory: The Journal of Physical Chemistry C, v. 120, n. 37, p. 20579–20587, https://doi.org/10.1021/acs.jpcc.6b00099

Evans, C. J., Nicholson, G. P., Faith, D. A., and Kan, M. J., 2004, Photochemical removal of uranium from a phosphate waste solution: Green Chemistry, v. 6, n. 4, p. 196–197, https://doi.org/10.1039/B313356G

Forouzan, F., Richards, T. C., and Bard, A. J., 1996, Photoinduced reaction at TiO_2 particles. Photodeposition from NiII solutions with oxalate: The Journal of Physical Chemistry, v. 100, n. 46, p. 18123–18127, https://doi.org/0.1021/jp953241f

Froideval, A., Del Nero, M., Barillon, R., Hommet, J., and Mignot, G., 2003, pH dependence of uranyl retention in a quartz/solution system: An XPS study: Journal of Colloid and Interface Science, v. 266, n. 2, p. 221–235, https://doi.org/10.1016/S0021-9797(03)00528-9

Gadd, G. M., 1999, Fungal production of citric and oxalic acid: Importance in metal speciation, physiology and biogeochemical processes: Advances in Microbial Physiology, v. 41, p. 47–92, https://doi.org/10.1016/S0065-2911(08)60165-4

Havel, J., Soto-Guerrero, J., and Lubal, P., 2002, Spectrophotometric study of uranyl–oxalate complexation in solution: Polyhedron, v. 21, n. 14–15, p. 1411–1420, https://doi.org/10.1016/S0277-5387(02)00947-6

Ilton, E. S., and Bagus, P. S., 2011, XPS determination of uranium oxidation states: Surface and Interface Analysis, v. 43, n. 13, p. 1549–1560, https://doi.org/10.1002/sia.3836

Ilton, E. S., Boily, J.-F., and Bagus, P. S., 2007, Beam induced reduction of U (VI) during X-ray photoelectron spectroscopy: The utility of the U4f satellite structure for identifying uranium oxidation states in mixed valence uranium oxides: Surface Science, v. 601, n. 4, p. 908–916, https://doi.org/10.1016/j.susc.2006.11.067

Kim, D., Duckworth, O. W., and Strathmann, T. J., 2009, Hydroxamate siderophore-promoted reactions between iron (II) and nitroaromatic groundwater contaminants: Geochimica et Cosmochimica Acta, v. 73, n. 5, p. 1297–1311, https://doi.org/10.1016/j.gca.2008.11.039

Kim, Y., Seo, J., Kang, S.-A., Choi, S.-G., and Lee, Y. J., 2015, Geochemistry and uranium mineralogy of the black slate in the Okcheon Metamorphic Belt, South Korea: Geochemical Journal, v. 49, n. 4, p. 443–452, https://doi.org/10.2343/geochemj.2.0369

Kim, Y. K., Lee, S., Ryu, J., and Park, H., 2015, Solar conversion of seawater uranium (VI) using TiO_2 electrodes: Applied Catalysis B: Environmental, v. 163, p. 584–590, https://doi.org/10.1016/j.apcatb.2014.08.041

Kubicki, J. D., Halada, G. P., Jha, P., and Phillips, B. L., 2009, Quantum mechanical calculation of aqueuous uranium complexes: Carbonate, phosphate, organic and biomolecular species: Chemistry Central Journal, v. 3, p. 10, https://doi.org/10.1186/1752-153X-3-10

Lucks, C., Rossberg, A., Tsushima, S., Foerstendorf, H., Fahmy, K., and Bernhard, G., 2013, Formic acid interaction with the uranyl (VI) ion: Structural and photochemical characterization: Dalton Transactions, v. 42, n. 37, p. 13584–13589, http://dx.doi.org/10.1039/C3DT51711J

Madden, T. H., Datye, A. K., Fulton, M., Prairie, M. R., Majumdar, S. A., and Stange, B. M., 1997, Oxidation of metal−EDTA complexes by TiO_2 photocatalysis: Environmental Science & Technology, v. 31, n. 12, p. 3475–3481, http://dx.doi.org/10.1021/es970226a

Morris, D. E., 2002, Redox energetics and kinetics of uranyl coordination complexes in aqueous solution: Inorganic Chemistry, v. 41, p. 3542–3547, http://dx.doi.org 10.1021/ic0201708

Noh, J. S., and Schwarz, J. A., 1989, Estimation of the point of zero charge of simple oxides by mass titration: Journal of Colloid and Interface Science, v. 130, n. 1, p. 157–164, https://doi.org/10.1016/0021-9797(89)90086-6

Perdew, J. P., Burke, K., and Ernzerhof, M., 1996, Generalized gradient approximation made simple: Physical Review Letters, v. 77, p. 3865, https://doi.org/10.1103/PhysRevLett.77.3865

Perron, H., Domain, C., Roques, J., Drot, R., Simoni, E., and Catalette, H., 2006, Periodic density functional theory investigation of the uranyl ion sorption on the TiO2 rutile (110) face: Inorganic Chemistry, v. 45, p. 6568–6570, https://doi.org/10.1021/ic0603914

Renock, D., Mueller, M., Yuan, K., Ewing, R. C., and Becker, U., 2013, The energetics and kinetics of uranyl

reduction on pyrite, hematite, and magnetite surfaces: A powder microelectrode study: Geochimica et Cosmochimica Acta, v. 118, p. 56–71, https://doi.org/10.1016/j.gca.2013.04.019

Salomone, V. N., Meichtry, J. M., Zampieri, G., and Litter, M. I., 2015, New insights in the heterogeneous photocatalytic removal of U (VI) in aqueous solution in the presence of 2-propanol: Chemical Engineering Journal, v. 261, p. 27–35, https://doi.org/10.1016/j.cej.2014.06.001

Schneider, S., Bister, S., Christl, M., Hori, M., Shozugawa, K., Synal, H.-A., Steinhauser, G., and Walther, C., 2017, Radionuclide pollution inside the Fukushima Daiichi Exclusion Zone, Part 2: Forensic search for the "forgotten" contaminants Uranium-236 and Plutonium: Applied Geochemistry, v. 85, Part B, p. 194–200, https://doi.org/10.1016/j.apgeochem.2017.05.022

Sobczyński, A., Duczmal, Ł., and Dobosz, A., 1999, Photocatalysis by illuminated titania: oxidation of hydroquinone and p-benzoquinone: Monatshefte für Chemie/Chemical Monthly, v. 130, p. 377–384.

Tsushima, S., Brendler, V., and Fahmy, K., 2010, Aqueous coordination chemistry and photochemistry of uranyl (VI) oxalate revisited: A density functional theory study: Dalton Transactions, v. 39, n. 45, p. 10953–10958, http://dx.doi.org/10.1039/C0DT00974A

Ulrich, K.-U., Ilton, E. S., Veeramani, H., Sharp, J. O., Bernier-Latmani, R., Schofield, E. J., Bargar, J. R., and Giammar, D. E., 2009, Comparative dissolution kinetics of biogenic and chemogenic uraninite under oxidizing conditions in the presence of carbonate: Geochimica et Cosmochimica Acta, v. 73, n. 20, p. 6065–6083, https://doi.org/10.1016/j.gca.2009.07.012

Vallet, V., Moll, H., Wahlgren, U., Szabó, Z., and Grenthe, I., 2003, Structure and bonding in solution of dioxouranium (VI) oxalate complexes: Isomers and intramolecular ligand exchange: Inorganic Chemistry, v. 42, n. 6, p. 1982–1993, https://doi.org/10.1021/ic026068s

Xu, Y., and Schoonen, M. A. A., 2000, The absolute energy positions of conduction and valence bands of selected semiconducting minerals: American Mineralogist, v. 85, n. 3–4, p. 543–556, https://doi.org/10.2138/am-2000-0416

Yang, J.-K., and Davis, A. P., 2000, Photocatalytic oxidation of Cu (II)− EDTA with illuminated TiO_2: Kinetics: Environmental Science & Technology, v. 34, n. 17, p. 3789–3795, https://doi.org/10.1021/es990874p

Yuan, K., Ilton, E. S., Antonio, M. R., Li, Z., Cook, P. J., and Becker, U., 2015, Electrochemical and spectroscopic evidence on the one-electron reduction of U (VI) to U (V) on magnetite: Environmental Science & Technology, v. 49, n. 10, p. 6206–6213, https://doi.org/10.1021/acs.est.5b00025

Yuan, K., Renock, D., Ewing, R. C., and Becker, U., 2015, Uranium reduction on magnetite: Probing for pentavalent uranium using electrochemical methods: Geochimica et Cosmochimica Acta, v. 156, p. 194–206, https://doi.org/10.1016/j.gca.2015.02.014